

Depth-PC: A Visual Servo Framework Integrated with Cross-Modality Fusion for Sim2Real Transfer

Haoyu Zhang¹, Weiyang Lin¹, Yimu Jiang¹, Chao Ye^{1✉}

Abstract—Visual servo techniques guide robotic motion using visual information to accomplish manipulation tasks, requiring high precision and robustness against noise. Traditional methods often require prior knowledge and are susceptible to external disturbances. Learning-driven alternatives, while promising, frequently struggle with the scarcity of training data and fall short in generalization. To address these challenges, we propose a novel visual servo framework *Depth-PC* that leverages simulation training and exploits semantic and geometric information of keypoints from images, enabling zero-shot transfer to real-world servo tasks. Our framework focuses on the servo controller which intertwines keypoint feature queries and relative depth information. Subsequently, the fused features from these two modalities are then processed by a Graph Neural Network to establish geometric and semantic correspondence between keypoints and update the robot state. Through simulation and real-world experiments, our approach demonstrates superior convergence basin and accuracy compared to state-of-the-art methods, fulfilling the requirements for robotic servo tasks while enabling zero-shot application to real-world scenarios. In addition to the enhancements achieved with our proposed framework, we have also substantiated the efficacy of cross-modality feature fusion within the realm of servo tasks.

I. INTRODUCTION

Given the current image, Visual Servo (VS) [1], [2] aims to guide the movement of robots for precise position control. To achieve this, robots need to automatically adjust their actions for desired control outcomes. Owing to its versatility and precision, VS has demonstrated significant potential across a wide range of applications, including industrial automation [3], visual navigation [4], and unmanned aerial vehicles [5]. Previous methods can be roughly categorized into two branches according to learning space within closed-loop control, undergoing a remarkable evolution: transitioning from image-based visual servo (IBVS) to position-based visual servo (PBVS).

Concretely, the camera-only solutions (also known as IBVS controllers) [6], [7], [8] control robots by minimizing the feature errors explicitly in the image space. This methodology can be traced back to keypoint correspondence between current and desired images, which promises robustness against the relative motion. On the other hand, PBVS controllers [9], [10], [11] incorporate camera calibration information for target’s location, which avoid explicit error correspondence and facilitate control within 3D space.

IBVS controllers are limited by a small convergence region and susceptibility to local minima, while PBVS ones are

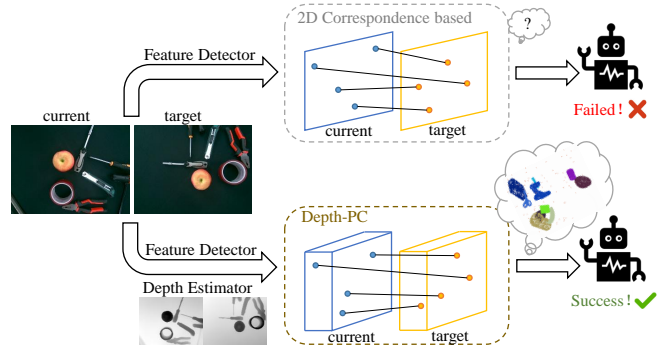


Fig. 1: Comparative visualization between visual servo methods based on 2D correspondence and ours.

prone to interference from relative motion [12]. Recent works such as CNS [18] utilize explicit correspondence with the neural policy to combine the both advantages. Additionally, NUVS [44] is designed to estimate the calibration embedding based on point correspondence. While highly effective, they are highly dependent on reliable matching of hand-crafted features from 2D space. This situation leads to a critical question: *the quality of the learned 2D correspondence features can not truly meet the requirement for effective Sim2Real transfer and precise 3D visual servo.*

In real world, environmental noise frequently interferes with systems’ ability to clearly perceive the spatial and geometric intricacies of objects within complex scenes. The reliance on 2D correspondence features alone is deficient in providing a comprehensive understanding of the scene, particularly when resolving 3D ambiguity and acquiring precise visual representations [41]. Numerous studies have delved into the pivotal role that depth information plays in robotic tasks [40], [41], [42]. They make great progress and demonstrate that usage of depth maps as input data effectively predicts the state of end-effectors. However, they are easily affected by the inaccuracy of depth maps, leading to the loss of spatial and geometric information.

In this research, we present an innovative framework **Depth-PC** that achieves zero-shot and Sim2Real effects by strategically decoupling the training and inference phases for the visual servo task. Instead of direct application of depth maps, we have opted to incorporate relative depth information to ensure a seamless alignment between 3D points of our simulation environment and those of the real world, addressing sim-to-real transfer challenges.

In the training stage, by extracting 2D coordinate features from sampled points, we fuse them with their respective

¹The authors are with Research Institute of Intelligent Control and Systems, Harbin Institute of Technology, Harbin, China

✉Corresponding author

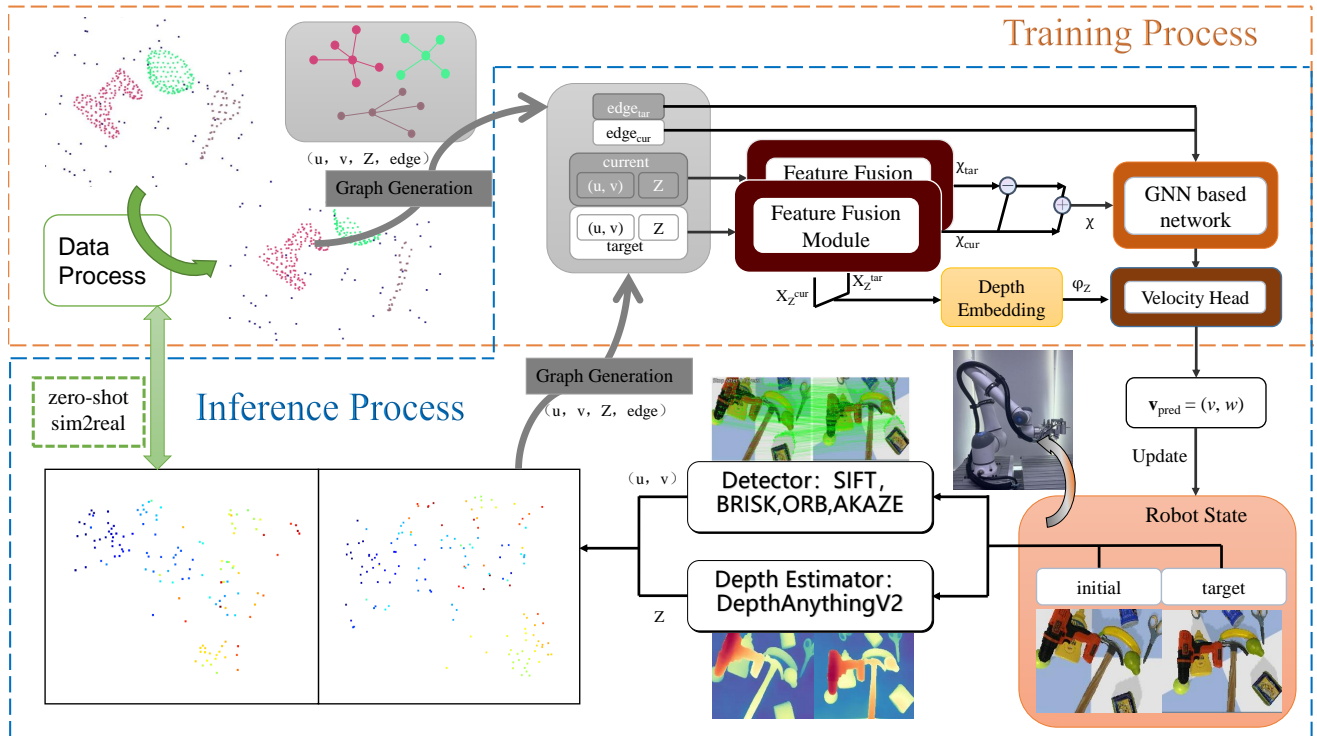


Fig. 2: Overview of our framework. The proposed framework is bifurcated into training and inference components. In the training phase, we primarily employ point clouds of objects that have been subjected to data process. In the inference phase, the inputs are derived from point clouds and depth information generated by a relative depth estimator. The features are then used to construct graph relationships, which produce 6-DOF velocity to guide the robot in executing servo tasks.

relative depths. Then they are then fed into a GNN [20] to establish correspondence between keypoints, yielding velocity of the end-effector to reach the intended destination. In the inference stage, we utilize a zero-shot depth estimator [33] to integrate relative depth features, which align with ones in simulation environment. The amalgamation of features capitalizes on the network’s spatial and geometric insights, and its inherent generalization capabilities. This sophisticated approach ensures the system’s enhanced capacity to precisely interpret the complex details within the environment and perform well across domains.

In summary, the contributions of our work are as follows:

- We have developed a novel framework for servo tasks, which achieves Sim2Real effectiveness by separating the training and inference processes. This approach aligns the simulation space with the real world, thereby extending generalizability to other scenarios in a zero-shot way.
- To our knowledge, we are the first to introduce cross-modal feature fusion into servo tasks. By leveraging a depth estimator and incorporating relative depth information, we further explore spatial and geometric features of point clouds, establishing correspondence for robotic applications.
- Our method’s excellence has been validated through zero-shot assessments conducted in both simulation environments and real-world scenes, demonstrating the superiority of our approach.

II. RELATED WORK

A. Traditional Visual Servo

Visual servo systems harness visual sensors to extract features from the frames, and calculate control directives to seamlessly steer the system toward its intended state. Traditional visual servo methodologies [1], [2] include IBVS, PBVS, and Hybrid Visual Servo. IBVS methods focus on leveraging geometric features directly derived from images [21]. It faces challenges such as unpredictable motion paths, potential Jacobian matrix singularities, local minima, and complications in feature extraction. On the other hand, PBVS [22] relies on 3D position data as visual cues, ensuring global asymptotic stability under perfect pose estimation conditions. But it necessitates prior knowledge like accurate camera parameters or 3D models of the target objects for estimating camera poses from images. Hybrid VS merges immediate image-level insights with reconstruction from dual viewpoints of a rigid object, decoupling rotation and translation [23], [24]. Nevertheless, this approach can escalate system complexity, challenging the integration and optimization of both features effectively.

B. Learning-based Visual Servo

Deep learning models excel in enhancing generalizability, precision, and adaptability. One pathway involves predicting the relative 6D orientation of objects, while the alternative strategy predicts the velocity of the end-effector to achieve the desired state.

Prior methods for 6D pose estimation often rely on instance-specific or category-level frameworks [14], [16], [26], necessitating CAD models of particular objects, and are limited to those specific cases. Generalization to novel instances or categories demands additional techniques, like NeRF [25], [16]. To counter these limitations, alternative approaches leverage depth information or point clouds, enriching the pose estimation with semantic cues. After initial pose estimation from rich reference perspectives, Gen6D [27] leverages a feature volume and neural networks for the refinement of the estimated poses. OnePose series [28], [29] employ SfM [30] to generate a sparse point cloud, aligning the target view with point clouds to ascertain the pose. Yet, these methods necessitate a multitude of annotated viewpoints, incurring significant costs. Ensuring real-time capability and precision during robotic manipulations further compounds the challenge.

Conversely, methods focusing on image features for velocity feedback have emerged. KOVIS [17] exemplifies this by training within simulation scenarios, harnessing supervised segmentation and depth information facilitating Sim2Real transfer for robotic manipulation tasks. Other techniques [13], [15], [31] concentrate on mapping current and target features to a latent space and utilizing an MLP as the predict head to output commands. While robust against intricate environments, these methods may not generalize seamlessly to new settings or adeptly manage rotation variances. CNS [18] enhances generalization by employing randomized simulated point clouds to forge feature correspondence, yet its performance wavers in noisy environments due to the absence of spatial and geometric insights.

C. Handling Depth in Visual Servo

Some works have delved into leveraging depth maps to construct servo systems. One such approach [40] utilizes depth maps of the robotic arm to directly estimate the angular joint positions. Another method [41] harnesses visual representations from color edges and learned depth keypoints, predicting the robotic state from the depth image. In addition to optical flow features, the approach [42] introduces depth information and employs the former for multi-perspective depth rectification. Nevertheless, these methodologies grapple with inherent issues such as the inaccuracy of depth in complex settings, limited convergence basins, and a lack of robust generalization across diverse scenarios. Essentially, while they aim to address the depth estimation problem, they do not offer tailored solutions for the intricacies of robotic control.

III. METHOD

Our objective is to perform servo tasks without the need for additional training ensuring the system’s flexibility to adapt seamlessly to a variety of scenarios in a zero-shot manner. We achieve this by training our network on randomized data generated through preprocess, while adopting a distinct approach for inference. To imbue the data with enriched spatial and geometric properties, and align the features of

simulation environment with those of real world, our approach incorporates dual tactics: 1). leveraging the "Hidden Points Removal" [34] operator and depth information that has been normalized; 2). crafting a feature fusion module designed to align depth data seamlessly with feature points. Besides, we integrate a relative depth estimation model [33] to facilitate the correspondence of depth features in the inference phase.

A. Data Processing

Our methodology is to generate data that is endowed with semantic and geometric information, an attribute that CNS [18] does not possess. For the 21 objects from YCB-Video, we integrate them into the simulation environment utilizing a stochastically determined quantity of point clouds.

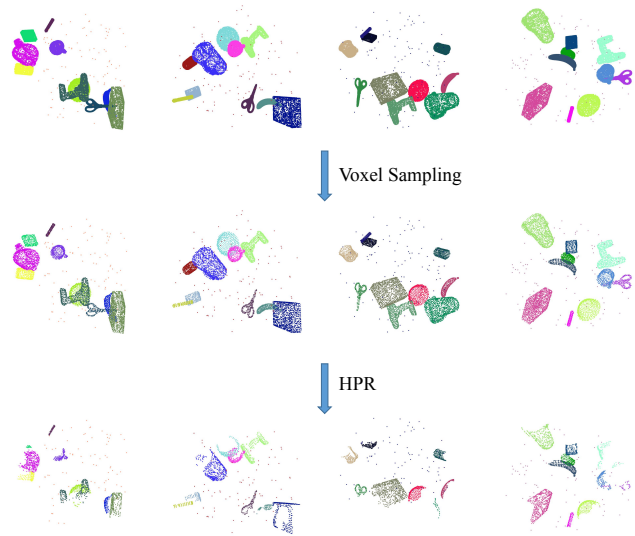


Fig. 3: Data Generation

Within this context, we establish a cylindrical spatial region $S(r, h)$ to encapsulate the loaded data sourced from the 3D models’ points clouds P^o . Given that the original models might encompass a substantial number of object point clouds $P_i^o \in P^o$ where $1 \leq i \leq N_c$, we initiate the process with voxel downsampling $V(\cdot)$ to make the following training simpler. This technique efficiently pinpoints the most representative surface points and concurrently curtails data volume, culminating in the refined point clouds cluster:

$$P_i^f = V(P_i^o) \quad (1)$$

Following this, each object is regarded as an individual cluster and there are N_c clusters. To enhance the dataset through augmentation, the positional centroids of these clusters are subject to randomization, and the clusters are respectively subjected to rotational transformations. Let us consider a 3D space populated with a total of N points and the i -th cluster is composed of n_i points, where both N and n_i are stochastically generated, ensuring that $\sum_{i=1}^{N_c} n_i < N$. For the i -th cluster, we randomly select n_i points by:

$$P_i = \{p_j \in P_i^f \mid 1 \leq j \leq n_i\} \quad (2)$$

The final points data has been obtained as $\mathcal{P} = \{\mathcal{P}_i \mid 1 \leq i \leq N_c\}$. This approach strikes a balance between the volume of data and the maximal extraction of semantic and geometric information from the data, a strategic decision that streamlines the training process.

Subsequently, we anchor our investigation on the spatial context previously delineated, meticulously sampling initial camera pose ${}^c_w T_i$ and target camera pose ${}^c_w T_t$. Leveraging these poses as pivotal reference points, we then implement the Hidden Points Removal $HPR(\cdot)$ technique to emulate the complexities of occlusions and visibility constraints encountered in the real world. For the points within the camera’s field of view, identify their boundaries R and subsequently apply the spherical flipping transformation:

$$\hat{p}_i = p_i + 2(R - \|p_i\|) \frac{p_i}{\|p_i\|}, p_i \in FOV \quad (3)$$

Next, calculate the convex hull for these points with the vertices of the hull pinpointing the essential data points we are interested in:

$$\hat{\mathcal{P}}_i = \{ConvHull(\hat{p}_j) \in \hat{\mathcal{P}} \cup {}^c_w t \mid 1 \leq j \leq n_i\} \quad (4)$$

The process is illustrated in Figure 3.

We project them onto the 2D camera plane (x, y) to serve as keypoints \hat{P} for practical applications. Subsequently, we normalize these coordinates in conjunction with the depth dimension Z , thereby transforming the data into a refined and standardized format. We further enrich the data’s diversity and robustness by **augmentation** : 1). randomly selecting a subset of points as mismatched entities; 2). randomly omitting certain points; 3). introducing noise that adheres to a uniform distribution.

Graph correspondence is generated among points (node embeddings), distinguishing between inter-cluster and intra-cluster connections. Initially, we designate the central point of each cluster as the cluster’s nucleus. Points that belong to the same cluster will be linked by edges, thereby creating the intra-cluster relationship matrix. The inter-cluster correspondence is articulated through the connections between the central points of different clusters. The graph structure, composed of node embeddings and edge embeddings, serves as the input for the network.

B. Feature Fusion Module

In order to enhance the spatial and geometric richness of the sampled points, we augment the data with the depth information, which is the distance from each point to the camera. Recognizing the profound efficacy of Cross Attention [35] in integrating multimodal features, as evidenced in various approaches, we employ it for feature fusion. We begin by mapping the normalized 2D feature points \hat{P}_{norm} and depth information Z_{norm} into a unified feature space, a process predominantly facilitated by FAL (Feature Alignment Layer), yielding feature points map and feature depth map:

$$X_{pos} = FAL(\hat{P}_{norm}), X_Z = FAL(Z_{norm}) \quad (5)$$

Despite its efficacy, Cross Attention suffers from high training cost, leading us to introduce Cluster Cross Attention.

For i -th cluster, we engage in the feature fusion process by first calculating the attention score matrix:

$$score^i = X_{pos}^i \cdot X_Z^T \in \mathbf{R}^{n_i \times N} \quad (6)$$

where n_i is the number of points in i -th cluster and N is feature dim.

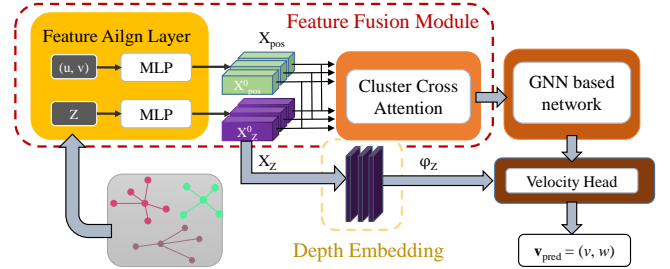


Fig. 4: Feature Fusion Module and Velocity Prediction

Subsequently, Softmax is applied to each row of the $score^i$ matrix to derive the attention matrix that represents the focus of depth information on coordinate information; similarly, the same operation is applied to each column to generate the attention matrix that encapsulates the attentive focus that coordinate information directs towards depth information.

$$\mathcal{A}_Z^i = \text{Softmax}_r(score^i), \mathcal{A}_{pos}^i = \text{Softmax}_c(score^i) \quad (7)$$

Ultimately, the updated fused features are obtained:

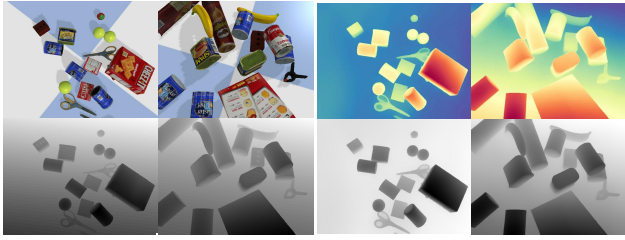
$$\mathcal{X}^i = [\mathcal{A}_Z^i \cdot X_Z^i, \mathcal{A}_{pos}^i \cdot X_{pos}^i] \quad (8)$$

This reciprocal cross-attention mechanism facilitates a mutual influence between keypoints features and depth information during updates, thereby boosting the expressive capacity of feature representations.

Besides, the depth branch of the fused features is fed into MLP, considered as depth embeddings φ_Z . This enhancement improves the controller’s capacity to capture spatial and geometric information, leading to more precise and responsive manipulation within the environment.

C. Training and Inference

Training Process While training exclusively on sampled points can improve the model’s generalization across diverse scenarios, we aim to expedite the convergence and enrich the model’s environmental understanding by integrating normalized depth information into the features. We follow the original method: 1). employing PointTransformerConv [36] and PointEdgeConv [37], [38] to perform intra-cluster and inter-cluster aggregation of feature points; 2). utilizing a velocity head to generate the end-effector’s 6 DOF decoupled velocity. Furthermore, we integrate depth embeddings into MLP, leveraging its robust feature extraction capabilities to refine the decoupled velocity. This approach injects structural and geometric knowledge into the model, thereby extending its adaptability to dynamic variations. Besides, GRU (Gated Recurrent Unit) [39] is employed to address the temporal issues associated with the dynamic motion of robots.



(a).simulation results (b).DepthAnythingV2 results

Fig. 5: Visualization of depth results. The figure on the left illustrates the depth maps rendered within the simulation environment, along with keypoint clouds detected; the figure on the right presents frames and keypoint clouds processed by the depth estimator. It is obvious that depth distributions of point clouds between them share a high degree of similarity.

Inference Process Due to the limitations of 3D cameras in reality, depth information is only effective within a certain range, and also greatly affected by external noise. Meanwhile, DINOv2 [19] demonstrates an exceptional ability to mine semantic information from images, leading to remarkable outcomes in relative depth estimation. This capability complements our normalized depth data, enabling the seamless alignment of semantic information between the simulation environment and real world, as shown in Figure 5. Consequently, we have integrated pre-trained DepthAnythingV2 [33] (DINOv2-based) in our experiments to ascertain relative depth information, constituting a vital component of our input data. Additionally, feature points can be obtained from any arbitrary keypoint detector, offering flexibility in our approach.

IV. EXPERIMENTS

Our experimental environments are divided into two parts: the simulation environment and the real-world environment. In both cases, we deploy our well-trained model to perform servo tasks in scenes where we randomly sample the initial and target poses. And images from the camera serve as input data for the network to directly predict the velocity of the robot’s end-effector, in a zero-short way. The evaluation criteria encompass success rate (SR), translation error (TE), rotation error (RE), time steps (TS) and mean total time cost on each run (mTT).

A. Simulation Environment

In the first scenario E_{YCB} rendered by PyBullet engine, we perform a comparative analysis with CNS [18] and IBVS [1] by introducing 3D models from the YCB dataset [14]. These levels are categorized into three types—S, M, L—based on their rotational deviation angles of 24.06° , 67.38° , and 136.46° , respectively. Each category is subjected to 50 iterative tests. We deem the servo task accomplished

when the final rotation is less than 3° and the translational accuracy is confined to a range of 3 cm.

TABLE I: We conduct experiments in E_{YCB} in a zero-shot way. And we consider the servo task to be successful when the mean points error is within the threshold and the state is maintained for 20 steps.

Method	SR(%)	TE(mm)	RE($^\circ$)	TS(0.04s)
IBVS[1]	85.33	1.602	0.136	253.9
RAFT[43]+IBVS	100	2.336	0.164	358.3
CNS[18]	100	1.592	0.134	207.8
Depth-PC(ours)	100	1.426	0.124	178.5

In this comparison, we all utilize AKAZE as the feature detector. The statistics clearly demonstrate a significant improvement of 15% in the convergence speed. Additionally, our model exhibits superior accuracy and notably outperforms other methods. We believe this is attributed to the depth feature injection, which enhances the model’s understanding of the geometric information in the environment.

For the second part, according to studies denoted by [18], [13] and [31], we adopt a similar approach of utilizing 2D images to construct task environment E_{image} . Data augmentation is applied to these images during training, including the introduction of occlusions, to simulate a more complex visual field. The network then analyzes perspectives from varied camera poses, providing a robust dataset for our model to predict actions accurately.

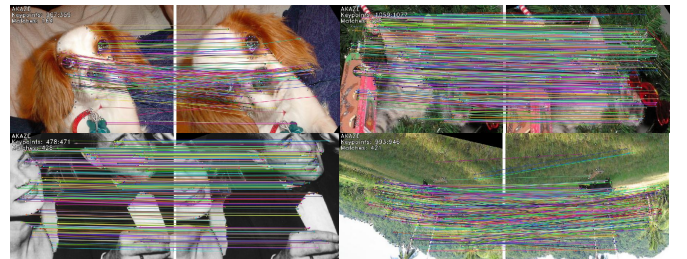


Fig. 6: Datasets in E_{image}

TABLE II: Experiments in E_{image} . The test images come from PASCAL VOC 2012, with pictures taken from different initial and target poses.

Method	SR(%)	TE(mm)	RE($^\circ$)	mTT(ms)
AlexNet-based[13]	93.20	28.854	2.365	401.0
Siame-se(3)[25]	92.67	54.084	6.758	401.0
CNS[18]	100	0.708	0.037	32.32
Depth-PC(ours)	99.33	0.626	0.124	32.06

Due to the specific training on certain datasets, methods such as [13] [31] have shown some effectiveness for specific datasets. Apart from the backbone, these methods relied solely on a simple MLP to predict the output velocities. However, by capitalizing on the broad generalization abilities of [18] and incorporating only the relative depth cues from images, we have managed to sidestep the constraints of varying scenes, thus attaining performance that is on par with existing SOTA.

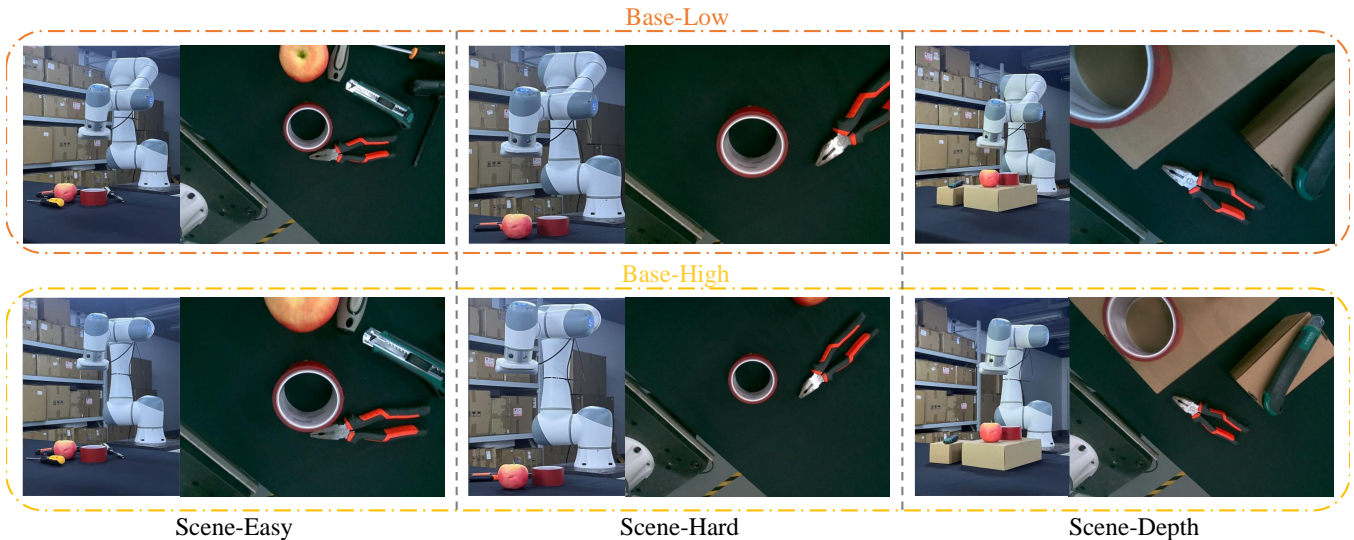


Fig. 7: Overview of varying degrees of proximity to the scene center for the robot’s end-effector across three distinct environments. The images on the upper side of each scene represent the situation where the robot is closer to the center of the scene, designated as Base-Low, while the ones on the lower row show the scenario where the robot is farther away, referred to as Base-High.

Our model’s comprehension of spatial and geometric information has yielded improved outcomes in terms of translation error and convergence rate. Nevertheless, the image transformations resulting from varied viewpoints can impact our understanding of the scene, particularly when depth information extends beyond the confines of the image boundaries.

B. Real World Environment

We have conducted comparative evaluations with CNS [18] and IBVS [1] within real-world settings. Basically, we categorized the scenarios into two distinct levels: Scene-Easy and Scene-Hard. Within each level, we sampled 50 pairs of initial and target poses, akin to the experimental setup employed by [18]. In the “Scene-Easy” setting, we introduce multiple objects to enhance the visibility of keypoints, thereby simplifying the servo control process. Conversely, in a more challenging environment, the number of objects is reduced, which increases the difficulty of the servo task at hand.

TABLE III: The results of the comparative experiments with IBVS and CNS in real world

Method	Scene-Easy			Scene-Hard		
	IBVS	CNS	Depth-PC(ours)	IBVS	CNS	Depth-PC(ours)
SR	38%	42%	60%	32%	38%	58%
TE(mm)	22.141	21.716	18.945	26.617	23.132	19.449
RE(°)	3.699	3.296	1.981	6.987	5.967	2.179
mTT(s)	6.010	6.743	4.021	8.002	8.409	4.874

The results demonstrate that our methodology has garnered superior results, with a **50%** improvement of SR, especially in complex settings and scenarios with substantial

depth variations. Our model notably excels at understanding geometric information of objects within 3D environment, thereby enhancing the servo task convergence rate—a finding that aligns with simulation outcomes. Concurrently, it maintains the precision of the model and bolsters its resilience against diverse levels of external noise, delivering a smoother motion trajectory.

C. Ablation Study

Initially, to assess the influence of data processing, we substitute the CNS method’s original data handling with our refined approach. The results clearly demonstrate that our data processing techniques, when substantially reducing the training cost, adeptly preserve the model’s precision. The training duration, which initially spans more than 5 hours, sees a reduction of nearly 20%.

TABLE IV: Ablation experiments on data processing and HPR represents our data processing approach. The statistics are derived from experiments carried out within E_{YCB} .

Method	SR(%)	TE(mm)	RE(°)	TS(0.04s)
CNS[18]+HPR	99.33	1.603	0.132	200.7
CNS	100	1.592	0.134	207.8
Depth-PC(w/o HPR)	99.33	1.592	0.137	185.1
Depth-PC(ours)	100	1.426	0.124	178.5

To evaluate the effectiveness of feature fusion module (FFM), we compare it with feature integration techniques like concatenation and Cross Attention, as TABLE V shown. FFM not only boosts servo task performance but also reduces resource usage. Specifically, while Cross Attention consumes 10GB of GPU memory for a batchsize of 16, our method maintains memory usage at 5~6GB even with a batchsize

of 64. This demonstrates that our approach has significant effects in multimodal feature fusion.

TABLE V: Ablation experiments on feature fusion module. The statistics are derived from experiments carried out within E_{YCB} .

Method	SR(%)	TE(mm)	RE($^{\circ}$)	TS(0.04s)
Depth-PC(Concat)	92.67	2.656	0.366	293.4
Depth-PC(Cross Attention)	96.67	1.794	0.147	228.2
Depth-PC(ours)	100	1.426	0.124	178.5

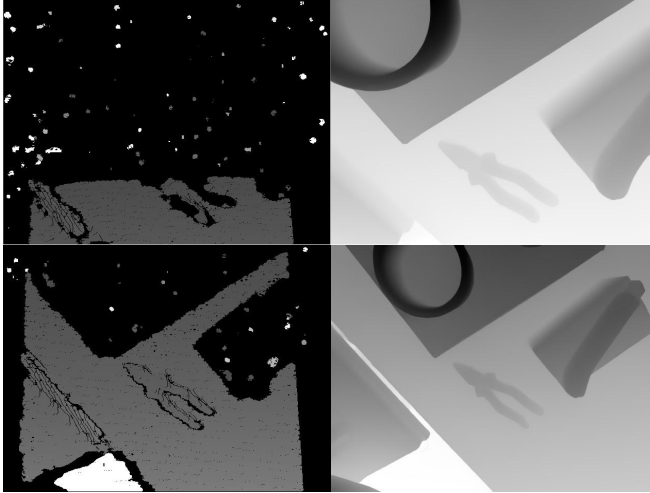


Fig. 8: Qualitative contrast between depth maps captured by the camera (left) and those estimated by the depth estimator (right) for Base-Low (upper) and Base-High (lower) in Scene-Depth.

Due to the fact that 3D cameras have fluctuating perception capabilities within different depth ranges shown as Figure 8, we have also carried out ablation studies across scenes that vary in distance from the scene center.

Specifically, we categorize tasks into Base-Low and Base-High based on the distance from the robot’s end-effector to the scene center. We then perform experiments across these scenes based on sources of depth maps, evaluating these acquired directly from cameras and those synthesized by the depth estimator

TABLE VI: The average results from ablation experiments on sources of depth maps in real world.

Method	SR(%)	TE(mm)	RE($^{\circ}$)	TS(s)
Depth-PC(Camera)	42.32	27.067	6.456	9.856
Depth-PC(ours)	59.67	18.720	3.156	6.006

It is clearly observable that when the camera on the robot’s end-effector is closer to the scene center, its interpretation of the environment’s geometric details is less accurate and more heavily impacted by noise. In contrast, the depth estimator demonstrates a robust ability to understand the scene effectively.

Furthermore, we have extended these two settings to three different environments as Figure 7: in addition to previously

TABLE VII: The average results influenced by the distance from the scene center across distinct experimental settings, shown as Figure 7.

Method	Base-Low			Base-High		
	IBVS	CNS	Depth-PC(ours)	IBVS	CNS	Depth-PC(ours)
SR(%)	38.67	43.33	62	31.33	36.67	57.33
TE(mm)	21.108	21.062	17.876	25.817	24.587	19.563
RE($^{\circ}$)	4.085	3.679	2.076	7.852	6.031	4.235
mTT(s)	6.893	6.632	5.136	9.658	8.974	6.876

mentioned Scene-Easy and Scene-Hard, we have introduced Scene-Depth, which encompasses objects at different depths.

The results clearly demonstrate that our model delivers more stable and precise performance in environments with substantial depth variations, and it exhibits an enhanced ability to generalize across various settings.

V. CONCLUSIONS

We develop a framework dedicated to servo tasks, which includes distinct processes for training and inference to achieve Sim2Real transfer in a zero-shot way. By integrating relative depth information, we facilitate cross-modal alignment and fusion between point clouds and the depth features of images. Furthermore, by employing feature detectors and depth estimators, we have narrowed the gap between the simulation environment and the real world, outperforming previous methodologies. In addition, we have delved into the effective fusion of multimodal features in visual servoing, and have successfully attained commendable outcomes in both performance and training costs. Our model has demonstrated robust capabilities and remarkable generalization across diverse complex environments, as evidenced by real-world experimental results.

REFERENCES

- [1] F. Chaumette and S. Hutchinson, “Visual servo control. i. basic approaches,” *IEEE Robotics & Automation Magazine*, vol. 13, no. 4, pp. 82–90, 2006.
- [2] S. Hutchinson, G. D. Hager, and P. I. Corke, “A tutorial on visual servo control,” *IEEE transactions on robotics and automation*, vol. 12, no. 5, pp. 651–670, 1996.
- [3] H. Nomura and T. Naito, “Integrated visual servoing system to grasp industrial parts moving on conveyor by controlling 6dof arm,” in *Smc 2000 conference proceedings. 2000 IEEE international conference on systems, man and cybernetics. cybernetics evolving to systems, humans, organizations, and their complex interactions’(cat. no. 0, vol. 3. IEEE, 2000, pp. 1768–1775.*
- [4] Y. Li and J. Kořecka, “Learning view and target invariant visual servoing for navigation,” in *2020 IEEE International Conference on Robotics and Automation (ICRA)*. IEEE, 2020, pp. 658–664.
- [5] N. Guenard, T. Hamel, and R. Mahony, “A practical visual servo control for an unmanned aerial vehicle,” *IEEE Transactions on Robotics*, vol. 24, no. 2, pp. 331–340, 2008.
- [6] A. Miranda-Moya, H. Castaneda, J. Gordillo, and H. Wang, “Ibvs based on adaptive sliding mode control for a quadrotor target tracking under perturbations,” *Mechatronics*, vol. 88, p. 102909, 2022.
- [7] S. R. Bista, P. R. Giordano, and F. Chaumette, “Appearance-based indoor navigation by ibvs using line segments,” *IEEE robotics and automation letters*, vol. 1, no. 1, pp. 423–430, 2016.
- [8] Y. Wang, Y. Yan, D. Shi, W. Zhu, J. Xia, T. Jeff, S. Jin, K. Gao, X. Li, and X. Yang, “Nerf-ibvs: visual servo based on nerf for visual localization and navigation,” *Advances in Neural Information Processing Systems*, vol. 36, 2024.

- [9] G. Dong and Z. Zhu, "Position-based visual servo control of autonomous robotic manipulators," *Acta Astronautica*, vol. 115, pp. 291–302, 2015.
- [10] S. Zhou, C. Shen, F. Pang, Z. Chen, J. Gu, and S. Zhu, "Position-based visual servoing control for multi-joint hydraulic manipulator," *Journal of Intelligent & Robotic Systems*, vol. 105, no. 2, p. 33, 2022.
- [11] P. Yu, N. Tan, and M. Mao, "Position-based visual servo control of dual robotic arms with unknown kinematic models: A cerebellum-inspired approach," *IEEE/ASME Transactions on Mechatronics*, vol. 28, no. 4, pp. 2328–2339, 2023.
- [12] J. Dong and J. Zhang, "A new image-based visual servoing method with velocity direction control," *Journal of the Franklin Institute*, vol. 357, no. 7, pp. 3993–4007, 2020.
- [13] Q. Bateux, E. Marchand, J. Leitner, F. Chaumette, and P. Corke, "Training deep neural networks for visual servoing," in *2018 IEEE international conference on robotics and automation (ICRA)*. IEEE, 2018, pp. 3307–3314.
- [14] Y. Xiang, T. Schmidt, V. Narayanan, and D. Fox, "Posecnn: A convolutional neural network for 6d object pose estimation in cluttered scenes," *arXiv preprint arXiv:1711.00199*, 2017.
- [15] C. Yu, Z. Cai, H. Pham, and Q.-C. Pham, "Siamese convolutional neural network for sub-millimeter-accurate camera pose estimation and visual servoing," in *2019 IEEE/RSJ International Conference on Intelligent Robots and Systems (IROS)*. IEEE, 2019, pp. 935–941.
- [16] B. Wen, W. Yang, J. Kautz, and S. Birchfield, "Foundationpose: Unified 6d pose estimation and tracking of novel objects," in *Proceedings of the IEEE/CVF Conference on Computer Vision and Pattern Recognition*, 2024, pp. 17 868–17 879.
- [17] E. Y. Puang, K. Peng Tee, and W. Jing, "Kovis: Keypoint-based visual servoing with zero-shot sim-to-real transfer for robotics manipulation," in *2020 IEEE/RSJ International Conference on Intelligent Robots and Systems (IROS)*, Oct 2020. [Online]. Available: <http://dx.doi.org/10.1109/iros45743.2020.9341370>
- [18] A. Chen, H. Yu, Y. Wang, and R. Xiong, "Cns: Correspondence encoded neural image servo policy," in *2024 IEEE International Conference on Robotics and Automation (ICRA)*. IEEE, 2024, pp. 17 410–17 416.
- [19] M. Oquab, T. Darcet, T. Moutakanni, H. Vo, M. Szafraniec, V. Khilodov, P. Fernandez, D. Haziza, F. Massa, A. El-Nouby *et al.*, "Dinov2: Learning robust visual features without supervision," *arXiv preprint arXiv:2304.07193*, 2023.
- [20] F. Scarselli, M. Gori, A. C. Tsoi, M. Hagenbuchner, and G. Monfardini, "The graph neural network model," *IEEE Transactions on Neural Networks*, p. 61–80, Jan 2009. [Online]. Available: <http://dx.doi.org/10.1109/tnn.2008.2005605>
- [21] A. A. Hafez, E. Cervera, and C. Jawahar, "Hybrid visual servoing by boosting ibvs and pbvs," in *2008 3rd International Conference on Information and Communication Technologies: From Theory to Applications*, 2008, pp. 1–6.
- [22] Z. Machkour, D. Ortiz-Arroyo, and P. Durdevic, "Classical and deep learning based visual servoing systems: A survey on state of the art," *Journal of Intelligent & Robotic Systems*, Jan 2022. [Online]. Available: <http://dx.doi.org/10.1007/s10846-021-01540-w>
- [23] R. Raja and S. Kumar, "A hybrid image based visual servoing for a manipulator using kinect," in *Proceedings of the Advances in Robotics*, Jun 2017. [Online]. Available: <http://dx.doi.org/10.1145/3132446.3134916>
- [24] C. Collewet and F. Chaumette, "Positioning a camera with respect to planar objects of unknown shape by coupling 2-d visual servoing and 3-d estimations," *IEEE Transactions on Robotics and Automation*, vol. 18, no. 3, p. 322–333, Jun 2002. [Online]. Available: <http://dx.doi.org/10.1109/tra.2002.1019462>
- [25] B. Mildenhall, P. P. Srinivasan, M. Tanckik, J. T. Barron, R. Ramamoorthi, and R. Ng, "Nerf: Representing scenes as neural radiance fields for view synthesis," *Communications of the ACM*, vol. 65, no. 1, pp. 99–106, 2021.
- [26] X. Chen, Z. Dong, J. Song, A. Geiger, and O. Hilliges, "Category level object pose estimation via neural analysis-by-synthesis," in *Computer Vision—ECCV 2020: 16th European Conference, Glasgow, UK, August 23–28, 2020, Proceedings, Part XXVI 16*. Springer, 2020, pp. 139–156.
- [27] Y. Liu, Y. Wen, S. Peng, C. Lin, X. Long, T. Komura, and W. Wang, "Gen6d: Generalizable model-free 6-dof object pose estimation from rgb images," in *European Conference on Computer Vision*. Springer, 2022, pp. 298–315.
- [28] J. Sun, Z. Wang, S. Zhang, X. He, H. Zhao, G. Zhang, and X. Zhou, "Onepose: One-shot object pose estimation without cad models," in *Proceedings of the IEEE/CVF Conference on Computer Vision and Pattern Recognition*, 2022, pp. 6825–6834.
- [29] X. He, J. Sun, Y. Wang, D. Huang, H. Bao, and X. Zhou, "Onepose++: Keypoint-free one-shot object pose estimation without cad models," *Advances in Neural Information Processing Systems*, vol. 35, pp. 35 103–35 115, 2022.
- [30] S. Ullman, "The interpretation of structure from motion," *Proceedings of the Royal Society of London. Series B. Biological Sciences*, vol. 203, no. 1153, pp. 405–426, 1979.
- [31] S. Felton, E. Fromont, and E. Marchand, "Siame-se (3): regression in se (3) for end-to-end visual servoing," in *2021 IEEE International Conference on Robotics and Automation (ICRA)*. IEEE, 2021, pp. 14 454–14 460.
- [32] N. Tumanyan, A. Singer, S. Bagon, and T. Dekel, "Dino-tracker: Taming dino for self-supervised point tracking in a single video," *arXiv preprint arXiv:2403.14548*, 2024.
- [33] L. Yang, B. Kang, Z. Huang, X. Xu, J. Feng, and H. Zhao, "Depth anything: Unleashing the power of large-scale unlabeled data," in *Proceedings of the IEEE/CVF Conference on Computer Vision and Pattern Recognition*, 2024, pp. 10 371–10 381.
- [34] S. Katz, A. Tal, and R. Basri, "Direct visibility of point sets," *ACM Trans. Graph.*, vol. 26, no. 3, p. 24–es, jul 2007. [Online]. Available: <https://doi.org/10.1145/1276377.1276407>
- [35] R. Hou, H. Chang, B. Ma, S. Shan, and X. Chen, "Cross attention network for few-shot classification," *Neural Information Processing Systems*, *Neural Information Processing Systems*, Sep 2019.
- [36] H. Zhao, L. Jiang, J. Jia, P. Torr, and V. Koltun, "Point transformer," in *2021 IEEE/CVF International Conference on Computer Vision (ICCV)*, Oct 2021. [Online]. Available: <http://dx.doi.org/10.1109/iccv48922.2021.01595>
- [37] R. Q. Charles, H. Su, M. Kaichun, and L. J. Guibas, "Pointnet: Deep learning on point sets for 3d classification and segmentation," in *2017 IEEE Conference on Computer Vision and Pattern Recognition (CVPR)*, Jul 2017. [Online]. Available: <http://dx.doi.org/10.1109/cvpr.2017.16>
- [38] Y. Wang, Y. Sun, Z. Liu, S. E. Sarma, M. M. Bronstein, and J. M. Solomon, "Dynamic graph cnn for learning on point clouds," *ACM Transactions on Graphics*, p. 1–12, Oct 2019. [Online]. Available: <http://dx.doi.org/10.1145/3326362>
- [39] J. Chung, C. Gulcehre, K. Cho, and Y. Bengio, "Empirical evaluation of gated recurrent neural networks on sequence modeling," *arXiv preprint arXiv:1412.3555*, 2014.
- [40] F. Widmaier, D. Kappler, S. Schaal, and J. Bohg, "Robot arm pose estimation by pixel-wise regression of joint angles," in *2016 IEEE International Conference on Robotics and Automation (ICRA)*. IEEE, 2016, pp. 616–623.
- [41] C. Rauch, V. Ivan, T. Hospedales, J. Shotton, and M. Fallon, "Learning-driven coarse-to-fine articulated robot tracking," in *2019 International Conference on Robotics and Automation (ICRA)*. IEEE, 2019, pp. 6604–6610.
- [42] Y. Harish, H. Pandya, A. Gaud, S. Terupally, S. Shankar, and K. M. Krishna, "Dfvs: Deep flow guided scene agnostic image based visual servoing," in *2020 IEEE International Conference on Robotics and Automation (ICRA)*. IEEE, 2020, pp. 9000–9006.
- [43] Z. Teed and J. Deng, "Raft: Recurrent all-pairs field transforms for optical flow," in *Computer Vision—ECCV 2020: 16th European Conference, Glasgow, UK, August 23–28, 2020, Proceedings, Part II 16*. Springer, 2020, pp. 402–419.
- [44] H. Yu, A. Chen, K. Xu, D. Guo, Y. Wei, Z. Zhou, X. Zhang, Y. Wang, and R. Xiong, "Adapting for calibration disturbances: A neural uncalibrated visual servoing policy," in *2024 IEEE International Conference on Robotics and Automation (ICRA)*. IEEE, 2024, pp. 17 417–17 423.